Argo float observations of basin-scale deep convection in the Irminger sea during winter 2011-2012

Piron Anne [1, *], Thierry Virginie [1], Mercier Herle [2], Caniaux Guy [3]

[1] Ifremer, Laboratoire de Physique des Océans, UMR 6523 CNRS-IFREMER-IRD-UBO, Plouzané, France
[2] CNRS, Laboratoire de Physique des Océans, UMR 6523 CNRS-IFREMER-IRD-UBO, Plouzané, France
[3] Centre National de Recherches Météorologiques/GAME, UMR 3589 Météo-France-CNRS, Toulouse, France

* Corresponding author : Anne Piron, Tel.: +33 2 98 22 42 83; fax: +33 2 98 22 44 96;
email address : vthierry@ifremer.fr

Abstract :

Analysis of Argo data obtained during winter 2011–2012 revealed the presence over the Irminger Basin of an exceptionally large number of profiles (41) with mixed layer depths (MLD) exceeding 700 m, which was deep enough to reach the pool of the intermediate Labrador Sea Water located in the Irminger Sea. Four of these profiles exhibited an MLD of 1000 m, which was the maximum value observed for the winter in question. The Argo sampling in the Irminger Sea during that winter, which was 3 to 4 times greater than for the preceding winters, enabled the different phases of the mixed layer deepening down to 1000 m, together with their spatial extents, to be observed for the first time. Two intense convective periods occurred: in late January south of Cape Farewell and in late February-early March east of Greenland. A final deepening period was observed in mid-March, during which the deepest mixed layers were observed. This long deepening period occurred in large regional areas and was followed by a rapid restratification phase. The temporal evolution of oxygen profiles from one Argo float testifies to the local and rapid ventilation of the mixed layer by the deep convection. A mixed layer heat budget along the trajectories of the 4 floats that sampled the deepest mixed layers showed that heat loss at the air-sea interface was mainly responsible for heat content variations in the mixed layer. Greenland Tip Jets were of primary importance for the development of deep convection in the Irminger Sea in the winter of 2011–2012. They enhanced the winter heat loss and two long (more than 24 hours), intense late events close together in time pushed the mixed layer deepening down to 1000 m. Net air-sea fluxes, the number of Greenland Tip Jets, the stratification of the water column, the NAO index and the Ekman-induced heat flux are pertinent indicators to assess conditions that are favorable for the development of deep convection in the Irminger Sea. By considering each of those indicators, it was concluded that the 2011-2012 event was not significantly different from the three other documented occurrences of deep convection in the Irminger Sea.

Highlights

► Exceptional Argo sampling in the Irminger Sea during winter 2011-2012. ► 41 profiles with MLD greater than 700 m; MLD of 1000 m for 4 of them. ► First description of the spatial extent of deep convection in the Irminger Sea. ► Heat loss at the air-sea interface main contributor to mixed layer deepening. ► Air-sea heat loss enhanced by Greenland Tip Jets and Ekman contribution.

1. Introduction

The Meridional Overturning Cell (MOC) is a key component of Earth's climate as it contributes to the redistribution of heat, salt and carbon within the world ocean. In the North- Atlantic Ocean, the warm and salty water masses of the upper limb of the MOC are progressively cooled and densified by convection. Convection is a mechanism related to the increase in surface density induced by heat loss and evaporation, leading to an increase in the

Mixed Layer Depth (MLD) (Lazier et al., 2001). In the subpolar gyre of the North-Atlantic Ocean, oceanic deep convection is the final stage of this continuous water-mass transformation process, in which intermediate and deep water masses are formed and feed the lower limb of the MOC. Deep convection not only provides dense water to the MOC but also helps to set the density of its lower limb. Given this relationship, we consider hereafter that convection in the North-Atlantic Ocean can be qualified as "deep" when it reaches the water masses of the MOC lower limb.

The two main sites of deep convection in the North-Atlantic are the Labrador Sea and the Greenland Sea (Lazier, 1980; Dickson et al., 1996). The Irminger Sea was also recognized as a possible site of deep convection by Nansen (1912) and Sverdrup et al. (1942) but this result was forgotten for decades because of a lack of observations, especially in winter (Pickart et al., 2003b, de Jong et al., 2012). In addition, under moderate forcing, the MLD in the Irminger Sea typically reaches 400 m (Centurioni and Gould, 2004, de Jong et al., 2012), which is not deep enough to reach the Labrador Sea Water (LSW) layer, the main intermediate water masses found in the Irminger Sea and belonging to the lower limb of the MOC (Lherminier et al., 2007). However, a decade ago, Pickart et al. (2003b) demonstrated that the conditions necessary for the development of deep convection are satisfied in the Irminger Sea by the presence of weakly stratified surface water, a closed cyclonic circulation and intense winter air-sea buoyancy fluxes (Marshall and Schott, 1999). Since then, a few observations of deep mixed layers have confirmed that the Irminger Sea is a deep convection site (Figure 1). Bacon et al. (2003) published measurements made by a profiling float south of Cape Farewell in March 1997 that showed a homogeneous density profile from the surface to more than 900 m. More recently, the analysis by de Jong et al. (2012) of the 2002-2010 time series from 2 moorings localized in the center of the Irminger Sea provided direct evidence of deep mixed layers. While the maximum MLD did not exceed 400 m during most winters, it reached 1000

3

and 800 m in the winters of 2007-2008 and 2008-2009, respectively. Indirect observations of convection with a homogeneous layer below a near-surface stratified layer were also reported. These profiles, referred to as isolated mixed layer in what follows, were observed in spring or in summer after the development of the shallow seasonal mixed layer. Using profiling floats and hydrographic sections, Bacon et al. (2003) and Våge et al. (2009a) reported such profiles southeast of Greenland in August-September 1997 and in the central Irminger Sea in April 2008, respectively. In both cases, the isolated mixed layer was observed down to about 1000 m. In April 1991, Pickart et al. (2003b) reported an isolated mixed layer south of Cape Farewell down to 1800 m, which is deeper than those observed in the 2000s. On the basis of various arguments, including an estimated advection time-scale, Pickart et al. (2003b) additionally concluded that the isolated mixed layers could not result from deep convection outside the Irminger Sea, in the central Labrador Sea for instance.
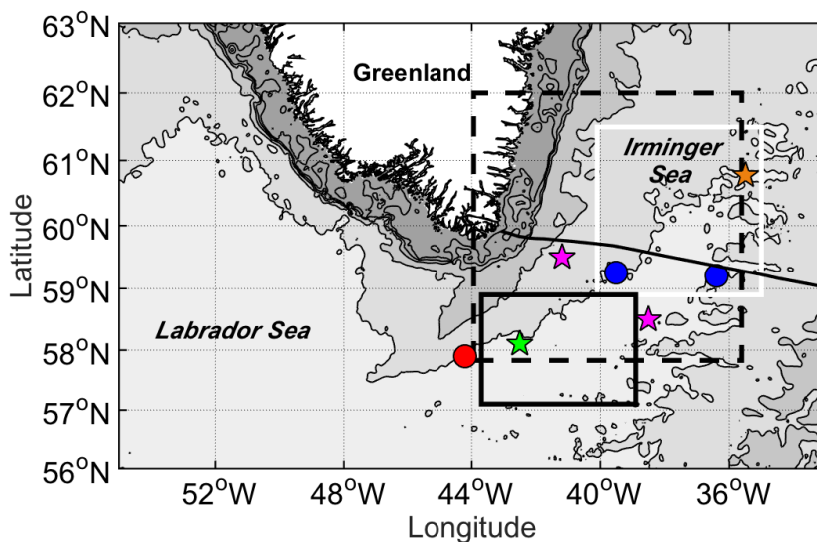

Figure 1: (Gray contours) Bathymetry of the Irminger and Labrador Seas. The isobaths are 200, 500, 1000, 2000, 3000 and 4000 m. The deep mixed layers observed in March 1997 (Bacon et al., 2003) (red dot) and in winters 2007-2008 and 2008-2009 (de Jong et al., 2012) (blue dots) are shown as well as the deep isolated mixed layers observed in

April 1991 (Pickart et al., 2003b) (green star), in August 1997 (Bacon et al., 2003) (pink stars) and in April 2008 (Våge et al., 2008) (orange star). The north, south and Tip Jet (TJ) boxes are represented by the white, black and dashed black lines, respectively. Hydrographic stations along the A25-Ovide line (Mercier et al., 2015) are represented by the black dots.

The magnitude of the winter air-sea heat loss and the preconditioning of the water column are essential elements controlling the intensity of the Irminger Sea convection (Pickart et al., 2003b; de Jong et al., 2012). The efficiency of the winter air-sea forcing to generate overturning depends on the number of Greenland Tip Jets that are regional-scale atmospheric events of high wind speed taking place to the east of the southern tip of Greenland (Doyle and Shapiro, 1999). The Greenland Tip Jets induce intense air-sea heat fluxes and wind-stress curl that act together to trigger intense mixing and deep convection in the Irminger Sea (Pickart et al., 2003a). Pickart et al. (2003a,b) established a relationship between deep convection in the Irminger Sea, the North-Atlantic Oscillation (NAO), which is the dominant mode of atmospheric variability in the North Atlantic sector (Hurrell, 1995), and the Greenland Tip Jets. A positive NAO index is expected to favor the occurrence of deep convection in the southwest Irminger Sea because Greenland Tip Jets are more frequent during winters with positive NAO index (Pickart et al., 2003a). However, according to Våge et al. (2009b), there is not a one-to-one correspondence between convection and the NAO index because other factors, such as preconditioning of the water column, are also important for regulating the depth of convection in the Irminger Sea.
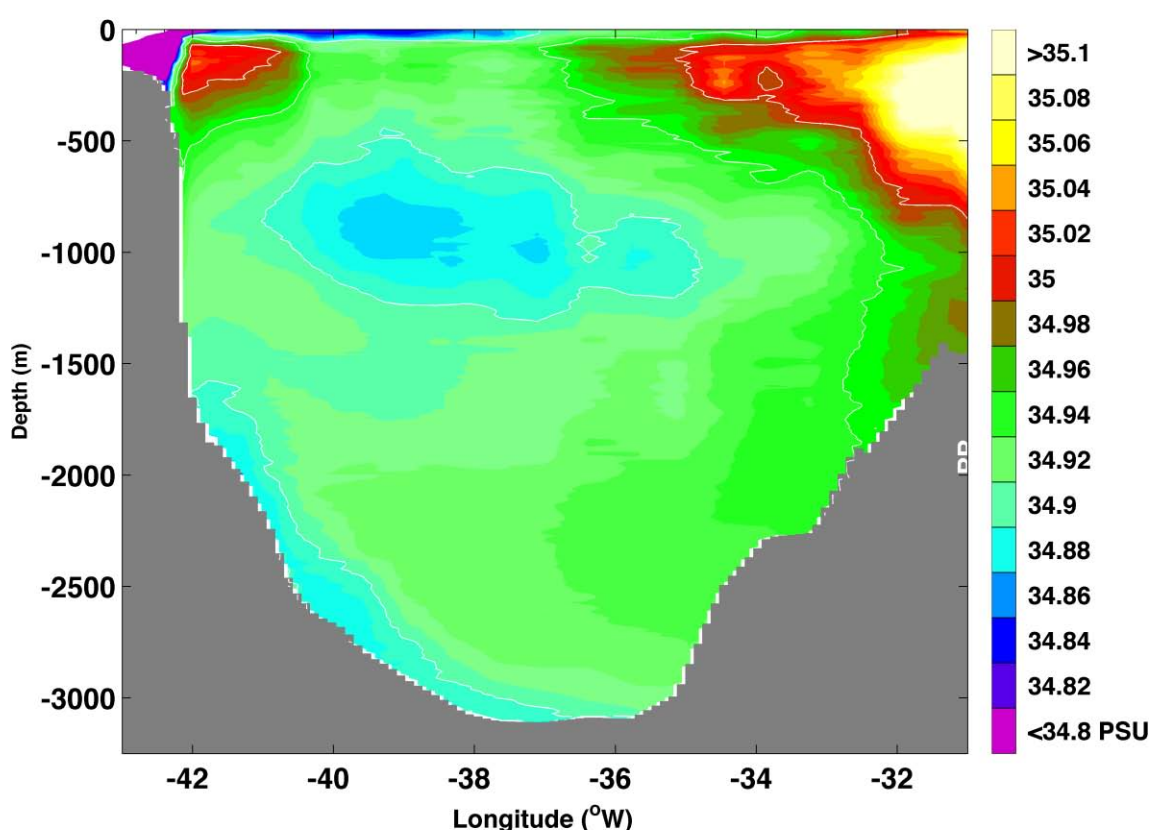
Figure 2: Salinity along the A25-Ovide line (see Figure 1) in the Irminger Basin averaged over the 6 hydrographic surveys carried out in June-July every 2 years from 2002 to 2012 (Mercier et al., 2015). The white contours represent the isohalines 34.9, 34.95 and 35. The LSW core is identified by the salinity minimum localized between about 700 and 1100 m depth and between 40 and 38°W.

During the last decade, only a small number of studies have shown that the Irminger Sea is a site for deep convection and investigated the mechanisms that could trigger such an event. Up to now, the description of a given event of deep convection has been limited by the available observations, which, themselves, were limited in space (one location) and time (one profile per year except for the moorings data analyzed by de Jong et al., 2012). Accordingly, the question that remains to be addressed is the following: What is the spatial extent of deep convection in the Irminger Sea? Thanks to the Argo program, it is now possible to answer this question. The Argo program provided exceptional sampling of the Irminger Sea in winter 2011-2012 and many of the profiles obtained showed MLDs greater than 700 m, which is the

upper limit of the LSW core in the Irminger Sea (Figure 2). Among those profiles, 4 exhibited MLDs down to 1000 m. The sampling in the Irminger Sea in winter 2011-2012 was 3 to 4 times greater than for the preceding winters. For instance, the number of profiles available between January and April in a box where the Greenland Tip Jets are the most intense (Våge et al., 2008, 2009b), and referred to in the following as the Tip Jet box (TJ box) (Figure 1), was 36 in 2012, whereas, on average over the period from 2002 to 2010, it was 9. Using atmospheric reanalyses and results of earlier studies, we investigated the forcing terms responsible for this occurrence of deep convection and compared them to those available in documented past occurrences of deep convection.

The paper is organized as follows. Section 2 presents the data used in this study, an evaluation of the air-sea fluxes, the methods of estimation of the MLD and the criterion employed to detect the occurrence of Greenland Tip Jets. The episode of deep convection during winter 2011-2012 in the Irminger Sea is described in detail in Section 3, with a focus on the spatial pattern and onset of the convective activity. Considering the mixed layer heat budget along the trajectories of 4 floats, we assess the main terms of the heat budget responsible for the mixed layer deepening and deep convection. Finally, the 2011-2012 winter is placed in an interannual context. Section 4 concludes the paper.

2. Data and methods

2.1. Argo data

Our study was based on the Argo dataset downloaded from the Coriolis Data Center (http://www.coriolis.eu.org) in October 2012 (no DOI was available at that time). We considered 1118 profiles from 68 Argo floats obtained between 52° and 66°N and between 44°W and the Reykjanes Ridge during the period from September 2011 to September 2012. The Argo floats provide data every 10 days on temperature (T), salinity (S) and pressure (P)

between 0 and 2000 dbar with a typical vertical resolution of 10 db in the upper layers and 25

db at depth. One float (WMO # 5902298) also measured dissolved oxygen concentration (O_2).

To obtain a heat budget along the trajectories of the 4 floats (WMO # 4901163, 4901165,

4901166 and 5902298) that detected the deepest MLDs for this winter (Section 3.2), the

vertical profiles of the 4 floats were linearly interpolated every 10 m from 5 to 1995 m.

Argo data undergo a careful quality control procedure including (1) real-time automatic test

and adjustment to assign a real-time quality flag and to provide real-time adjustment

whenever possible (Wong et al., 2014), (2) delayed-mode adjustment following Owens and

Wong (2009), and (3) a final quality check of the basin-scale consistency of the Argo data as

part of the Argo Regional Center dataset (Gaillard et al., 2009). Good and probably good (QC

flag 1 or 2) Argo data were used in this study. When available, the adjusted field was used. O_2

data from float WMO # 5902298 were corrected with respect to a reference profile collected

at float deployment following Takeshita et al. (2013). Overall, the accuracy of the data was

$0.01°C$, 0.02, 5 dbar and 8 μmol kg^{-1} for T, S, P and O_2, respectively.

2.2. Mixed Layer Depth estimation

The study was based on the determination of MLD from Argo profiles. In order to ensure a

robust estimation of the MLDs, three methods were used: the "threshold method" used by de

Boyer Montégut et al. (2004), the "split-and-merge method" proposed by Thomson and Fine

(2003) and a visual inspection as proposed by Pickart et al. (2002). The threshold method is

based on a density difference between the surface and the base of the mixed layer. Simple to

implement, this method has been used in many studies. However the density threshold of 0.03

kg m^{-3}, used by de Boyer Montégut et al. (2004) in establishing their world climatology,

overestimated MLD values in the Irminger and Labrador Seas by up to several hundred

meters (Figure 3a). Based on a visual inspection of a subset of the profiles, a new threshold

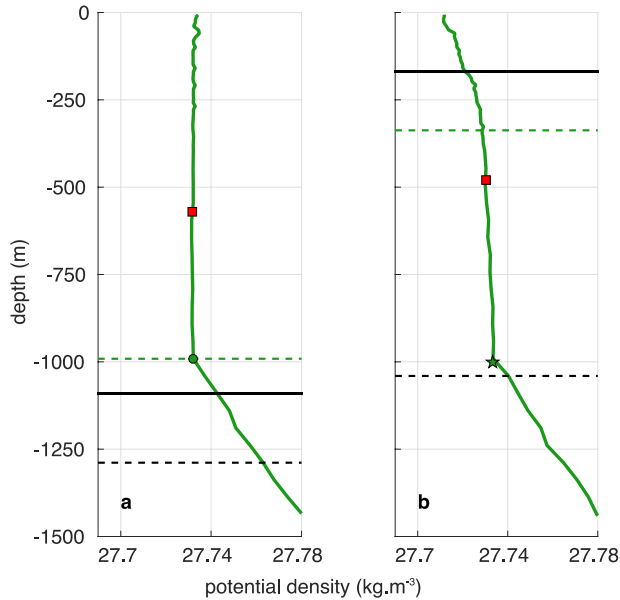value of 0.01 kg m^{-3} was determined for those basins.

Figure 3: Example of MLD estimation for 2 profiles collected in the Irminger Sea. (a) Typical vertical profiles observed in the winter of 2011-2012. (b) Typical profiles observed in spring 2012 after the beginning of restratification. (Thick, colored lines) Potential density in kg m^{-3}. (Dashed-dotted, colored horizontal lines) MLD estimation from the split-and-merge method with an error criterion of 0.003 kg^2 m^{-6}. (Black horizontal lines) MLD estimation from the threshold method with a density criterion of 0.01 kg m^{-3}. (Dashed black horizontal lines) MLD estimation from the threshold method with density criterion of 0.03 kg m^{-3}. (Dots or stars) Final estimation of the depth of the mixed or homogeneous layer. (Red squares) Depth at which the potential vorticity was minimum and where the thermohaline properties of the MLD were estimated.

The split-and-merge method is based on the approximation of the profile by a suite of first

order polynomials (segments) obtained by minimizing the number of segments while keeping

the error ε between the real profile and the approximated profile below a given threshold. The

MLD is defined as the base of the first segment. The maximum error ε_{max} that should not be

exceeded is the criterion that must be chosen by the user. Using an analysis of variance

(ANOVA; Wu and Hamada, 2000) that compared the split-and-merge method with the

threshold method, we established that the most suitable criterion for MLD estimation with the split-and-merge method in the Labrador and Irminger Seas was $\varepsilon_{max} = 0.003$ kg^2 m^{-6}.

MLD determination based on a visual inspection of the profiles is the most accurate method, especially in the weakly stratified subpolar gyre of the North-Atlantic Ocean, but it is inappropriate when dealing with a large number of profiles. For this reason, the MLD for each profile of our dataset was first automatically estimated following the threshold and split-and-merge methods. The MLD value was verified by a visual inspection of the corresponding profile when the two estimates differed (Figure 3a), when it was inconsistent with that of nearby profiles or when it was unexpected or exceptionally large. In the following, we consider that an MLD greater than 700 m is the signature of deep convection in the Irminger Sea since it indicates ventilation of the lower limb of the MOC (Section 1).

Some of the winter profiles presented a deep homogeneous layer exceeding 700 m below a stratified surface layer. If the comparison with neighboring profiles in space and time indicated that the stratified near-surface layer was recent due, for instance, to recent horizontal intrusion of near surface stratified layers, we considered that the deep homogeneous layer represented a recent mixing event. The MLD was thus set at the base of this deep homogeneous layer. During the restratification phase in spring, some isolated mixed layer profiles also presented a deep homogeneous layer exceeding 700 m (Figure 3b), which will be referred to as a deep isolated mixed layer. Finally, the properties (potential temperature, salinity and potential density) of the deep mixed layers and of the deep isolated mixed layers observed during the restratification phase were calculated in a similar way, at the potential vorticity minimum (Figure 3).

2.3. Wind data and Greenland Tip Jet detection

10

Wind and wind-stress used in this study came from the ERA-Interim reanalysis (Dee et al., 2011) from the European Centre for Medium-Range Weather Forecasts (ECMWF). The fields were available every 12 hours at a horizontal resolution of 0.5 ° in longitude and latitude.

According to Renfrew et al. (2009), the ability of different atmospheric analyses to reproduce the surface fields associated with high winds such as Greenland Tip Jets depends on various model parameters, such as model resolution, surface flux parameterization or atmospheric surface layer scheme. These authors compared the ability of different data sets, including the ERA-40 atmospheric reanalysis from ECMWF (Uppala et al., 2005) and the NCEP reanalysis, to reproduce the surface fields at the Denmark Strait and in the Irminger Sea. They showed that the ERA-40 reanalysis produced turbulent surface fluxes in reasonable agreement with observations. Since then, the ERA-Interim atmospheric reanalysis has been released (Dee et al., 2011). An improved assimilation scheme and a better horizontal resolution are examples of important improvements made to this reanalysis.
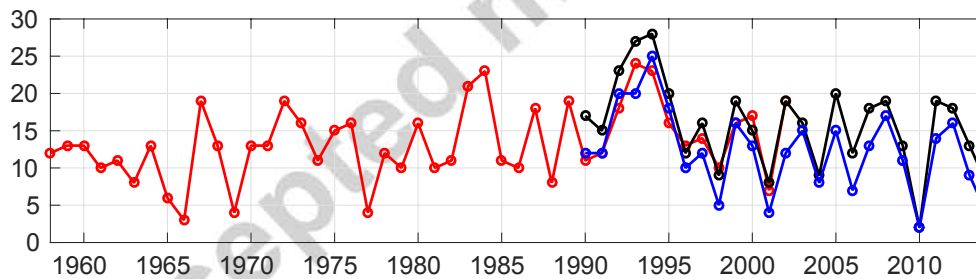

Figure 4: (Red curve) Time series from 1958 to 2001 of winter (from November to April) Greenland Tip Jet frequency as obtained by Våge et al. (2009b) and based on the 6 hourly ERA-40 dataset and a Tip Jet criterion of 18 m s^{-1}. (Black and Blue curves) Time series from 1990 to 2014 for winter (from November to April) Greenland Tip Jet frequency based on the 12 hourly ERA-Interim dataset and a TJ criterion of 18 m s^{-1} and 19 m s^{-1}, respectively. The year indicated in the time axis corresponds to the year at the end of winter.

We compared ERA-Interim winds with ASCAT (Advanced SCATerometer) wind fields provided by the MetOp satellite (Bentamy et al., 2008) in the TJ box over the period 1 November 2011 – 31 March 2012 (not shown). We did not use ASCAT gridded products (1/4° horizontal resolution) because they are available as a daily mean, which is not sufficient to represent Greenland Tip Jets, whose temporal scale is generally less than 1 day (Våge et al., 2009). We thus used along-track ASCAT data. Note that the 2 datasets are not independent since the ASCAT data are assimilated in ERA-Interim. In agreement with Harden et al. (2011), ERA-Interim wind speed was found to be slightly underestimated compared to ASCAT wind speed (by 1-2 m s^{-1}) for moderate wind speed (less than 20 m s^{-1}). As with the ERA-40 reanalysis (Våge et al., 2009b), a threshold effect appeared at high wind speed: the ERA-Interim wind speed never exceeded 27 m s^{-1} while ASCAT wind speed reached values greater than 35 m s^{-1}. Despite these limitations, agreement between ASCAT data and ERA-INTERIM was good overall. Since the ASCAT data did not have the necessary resolution for Greenland Tip Jet detection, ERA-INTERIM was used for this purpose. The criterion was based on the zonal wind speed averaged in the TJ box and was designed to provide results similar to those obtained by Våge et al. (2009b) for the period 1958-2002. Using 12-hourly ERA-interim winds, the best agreement with Våge et al. (2009b) was given by using a zonal wind speed averaged in the TJ box greater than 19 m s^{-1} (Figure 4) after 1995 and greater than 18 m s^{-1} in the early 1990s. As using 18 or 19 m s^{-1} did not significantly affect our results, we used the criterion that provided the best agreement over the whole common period (1992-2002), which was 19 m s^{-1}. The Greenland Tip Jet detection was considered over 1990-2012 in order to put the winter of 2011-2012 in an interannual context.

2.4. Air-sea heat fluxes and SST

Net air-sea heat fluxes and sea surface temperatures (SST) were taken from the ERA-Interim reanalysis at the same spatial and temporal resolution as the wind fields (see Section 2.3).
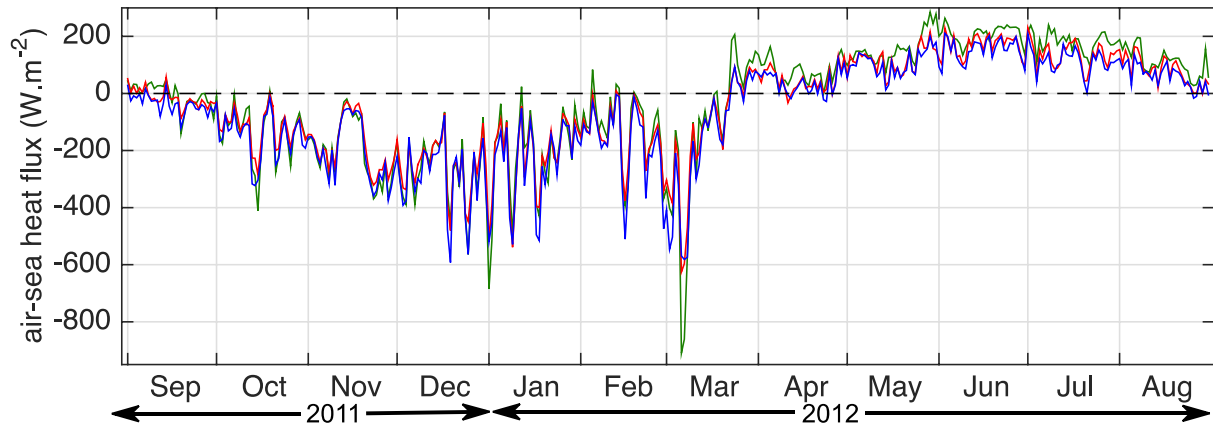
12

Figure 5: Time series of the net air-sea heat fluxes averaged over the TJ box from NCEP (green curve), ERA-Interim (red curve) and ARPEGE (blue curve) between 1 September 2011 and 31 August 2012. Positive values represent heat gain by the ocean.

ERA-Interim net air-sea heat fluxes were used preferentially in this study as they had been validated against observations in this region before with good results (Renfrew et al., 2009; Harden et al., 2011). Net air-sea heat fluxes from the numerical weather prediction model ARPEGE (Action de Recherche Petite Echelle Grande Echelle) (Déqué et al., 1994) and from NCEP (National Centers for Environmental Prediction) Reanalysis 2 (Kanamitsu et al., 2002) were also used to verify the robustness of our results. Both fields were available at 1/2° horizontal resolution and as a daily mean. The comparison was made in the TJ box (Figure 5). The mean and rms differences between ERA-Interim data and ARPEGE (or NCEP) data were 22.9 and 36.1 W m^{-2}, respectively (or -13.8 and 49.7 W m^{-2}, respectively). Most importantly for our study, the correlation between the time series was remarkably high (more than 98% in both cases), with heat loss peaks detected at the same dates with the 3 products, especially during winter. However some differences affected the amplitudes of the stronger events. For instance, the NCEP model provided more extreme values (positive or negative) than ERA-Interim and ARPEGE.

2.5. Absolute Dynamic Topography

Absolute Dynamic Topography (ADT) data provided by AVISO (Archiving Validation

Interpretation Satellites Oceanographic data; http://www.aviso.oceanobs.com/duacs/) were

used in this study (Section 3) to visualize the intensity and delimit the location of the Irminger

Gyre (Våge et al., 2011) and as an indicator of the preconditioning of the water column (de

Jong et al., 2012). ADT fields have been available every 7 days since October 1992 with a

horizontal resolution of 1/3°. During February-March 2012, ADT fields were available at the

following dates: 22 and 29 February and 7, 14, 21, 28 March 2012.

3. Basin-scale deep convection in the Irminger Sea during winter 2011-2012

3.1. Temporal evolution and spatial extent

Analysis of MLDs during winter 2011-2012 revealed the presence of an exceptionally large

number of profiles (41) over the Irminger Basin with MLDs exceeding 700 m. Such mixed

layers are qualified as "deep" in what follows. Among them, 4 profiles exhibited an MLD of

1000 m (Figure 6, Figure 7b), which was the maximum value observed for the winter

analyzed. A large number of spring profiles (17) also presented an isolated mixed layer

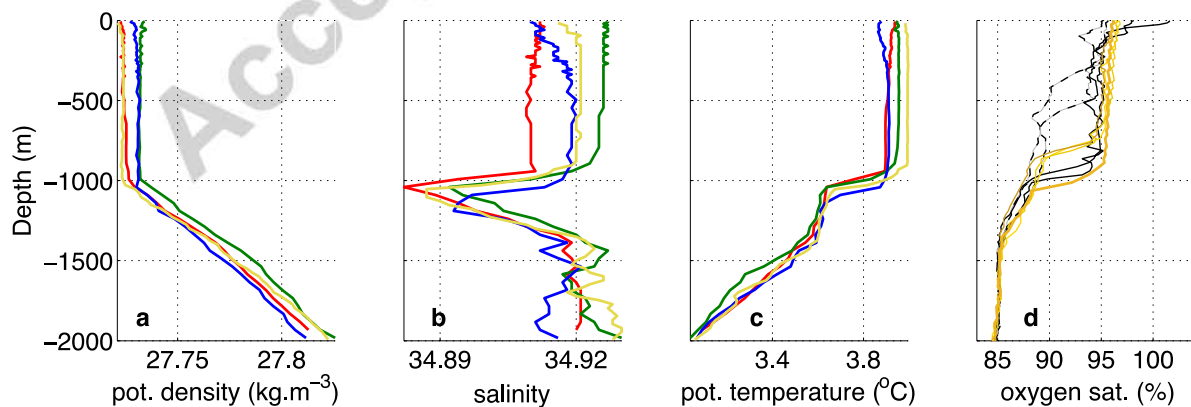deeper than 700 m, 5 of which reached 1000 m (Figure 7b).

Figure 6: Potential density (kg m^{-3}) (a), salinity (b), and potential temperature (°C) (c) profiles from floats 4901163 (red), 4901165 (green), 4901166 (blue) and 5902298 (yellow) with an MLD of about 1000 m. Oxygen saturation (%) profiles (d) from float 5902298 on 30 January and 18 February (black dashed lines), on 19 February, 29 February, 10 March and 20 March (yellow lines) and on 30 March and 9 April (black lines) 2012.

The MLD evolution during winter 2011-2012 is first described along the trajectories of the floats 4901163, 4901165, 4901166 and 5902298 (Figure 7a), which exhibited the deepest MLD values during this period. While float 5902298 remained in the Irminger Sea (east of 44°W) during the whole period, the other three floats were located in the Labrador Sea in September 2011. These three floats followed a similar pathway while traveling toward the Irminger Sea but with different timing. They entered the Irminger Sea at the end of October 2011 (4901163), end of December 2011 (4901165) and end of January 2012 (4901166), where they remained until the end of the winter. The mixed layer deepening was synchronous for the 4 floats and occurred from early November 2011 to mid-March 2012 (Figure 7b). It ended abruptly and simultaneously for the 4 floats after mid-March with the onset of the spring restratification characterized by the presence of a near-surface stratified layer above a deep homogeneous layer (Figure 7b).
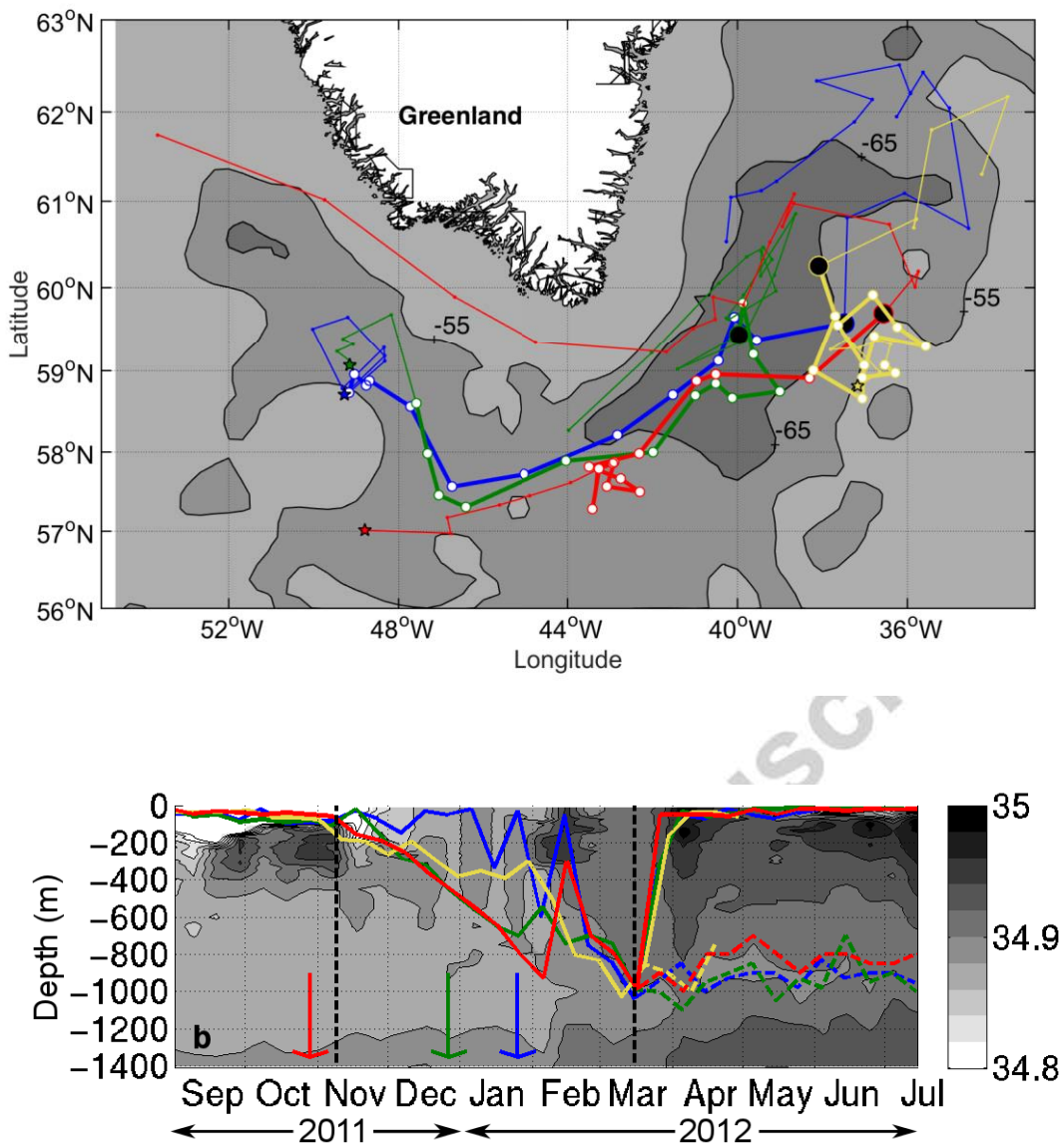
Figure 7: (a) ADT contours (-55 and -65 cm) on 14 March 2012 and trajectories of floats 4901163 (red line), 4901165 (green line), 4901166 (blue line) and 5902298 (yellow line) between 1 September 2011 and July 2012. The first position is represented by a star. White dots represent profile positions during the MLD deepening phase (see (b)) and black dots represent the positions of the 1000 m MLD. (b) MLD time series for floats 4901163 (red line), 4901165 (green line), 4901166 (blue line) and 5902298 (yellow line) between 1 September 2011 and July 2012. The colored dashed lines represent the depth of the homogeneous layer observed below the near-surface stratified layer in spring. The black dashed lines delimit the deepening period, which was similar for the 4 floats (9 November 2011 - 16 March 2012). Arrows indicate when each float entered the Irminger Sea (east of 44°W). The contours represent salinity values on a section along the trajectory of float 4901163.

The deep convection observed during winter 2011-2012 is now further described by considering horizontal maps indicating the positions of the profiles with deep mixed layers (Figure 8). The deep mixed layers were observed over a large area extending from the south of Cape Farewell to the central part of the Irminger Sea and bounded by the -55 cm ADT contour that defines, in agreement with Våge et al. (2011), the Irminger Gyre. They were generally observed within or to the east of the Irminger Gyre core, which is defined by the -65 cm ADT contour. These maps allow the following chronology of the event to be described:

1. No profile with a deep mixed layer was observed before 18 January 2012. From 18 January to 3 February 2012, 45% of the profiles located inside the Irminger Gyre had an MLD greater than 700 m (Figure 8a). This ratio increased to 69% (9 out of 13 profiles) when profiles south of 61°N were considered. Most of the deep mixed layer profiles (8 out of 9) were localized south of Cape Farewell in the southern part of the Irminger Gyre, in an area referred to as the south box below (Figure 8). Profiles with the deepest mixed layers observed during this period (800 m) were localized in this box. One profile with a deep isolated mixed layer was also observed east of Greenland in the area referred to as the north box but, because of a lack of data, it was not possible to know whether there was continuity between those two areas or not.

2. From 4 February to 20 February 2012, a similar number of deep mixed layers were observed within the Irminger Gyre (9 profiles) but represented a lower proportion (30% of the profiles) compared to the previous period. Those profiles were located to the east of the core of the Irminger Gyre (Figure 8b), which was narrower than in the previous and following periods. This suggests that, during this period, the deepening slowed down compared to the previous period.

3. From 21 February to 8 March, 46% (11 out of 24) of the profiles localized inside the Irminger Gyre had an MLD greater than 700 m (Figure 8c). Profiles with a deep mixed layer were observed further north than in the first period. Most of them were observed east of Greenland in the north box (Figure 8c,e), except for one that was located south of 58°N. During this period, the deepest mixed layers reached 850 m east of Greenland.

4. A final deepening phase then occurred between 9 and 25 March 2012. During that period, 60% of the profiles (12 out of 20) exhibited a deep mixed layer. All of them had an MLD greater than 800 m. Those profiles were localized east and south of Greenland; 8 were in the north box, while 3 were in the south box. Between 9 and 16 March 2012, 4 profiles in the north box exhibited MLDs of about 1000 m (Figure 8d,e) while the most western profile in the south box exhibited an MLD of 950 m. The extent of the core of the Irminger Gyre (ADT contour of -65 cm) was as large as in the previous period and larger than in the other three periods. As will be shown in Section 3.3, the ADT value averaged in the two boxes reached a minimum during this period. The deepening period stopped abruptly after 25 March 2012.

5. During the next 17 days, no profiles with a deep mixed layer were observed and 58% (14 out of 24) of the profiles were characterized by an isolated mixed layer deeper than 700 m, 5 of which even reached 1000 m (Figure 8f).

Our dataset revealed that the deepening of the mixed layer occurred in large regional areas. We observed a deepening of the mixed layer south of Cape Farewell down to 800 m in late January and a deepening down to 1000 m east of Greenland in late February. The hypothesis that the mixed layer deepening occurred simultaneously over a single large area extending from south of Cape Farewell to the northern part of the Irminger Gyre, as suggested by the few profiles exhibiting deep mixed layers east of Greenland in January and south of Cape Farewell in late February-mid March, cannot be excluded. The deep profiles were generally

observed within or to the east of the Irminger Gyre core. The lack of deep profiles to the west of the Irminger Gyre core might be due to a sampling bias but physical processes, like the presence of the warm and salty Irminger water flowing southward with the East Greenland/Irminger Current (Pickart et al., 2005, Figure 2) might also be involved. This reveals that despite the exceptional sampling of the Irminger Sea during the winter of 2011-2012 by Argo floats, an even denser and more uniform sampling would be needed for a full description of the spatial pattern resulting from deep convection events in the Irminger Sea.
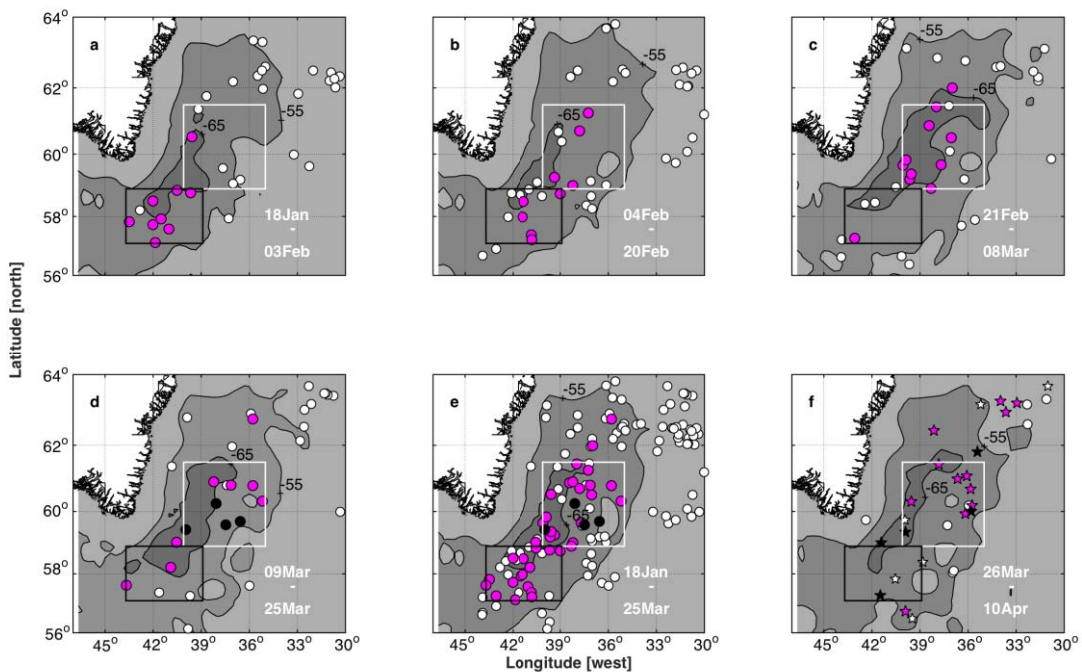

Figure 8: Argo profile positions in the Irminger Sea over (a) 18 January to 03 February 2012; (b) 04 February to 20 February 2012; (c) 21 February to 08 March 2012; (d) 09 March to 25 March 2012; (e) 19 January to 25 March 2012; (f) 26 March to 10 April 2012. MLDs less than 700 m are plotted as circles filled in white, MLDs greater than 700 m are in magenta and MLDs equal to about 1000 m are in black. Stars represent profiles with a homogeneous layer deeper than 700 m below a stratified near-surface layer. Contours are Absolute Dynamic Topography (ADT) averaged over the period covered in each panel. The isolines correspond to the -55 and -65 cm contours. The black and white boxes are the south and north boxes, respectively.

The deep mixed layers and the deep isolated mixed layers were warmer and saltier in the north box than in the south box (Figure 9). The properties in the north box at the end of the convective period, which ranged between 3.85 and 4.15°C and between 34.91 and 34.95 (Figure 6 and Figure 9), were similar to those found by de Jong et al. (2012). In the south box, the properties at the end of the convective period ranged between 3.65 and 4°C and between 34.86 and 34.91. Temperature and salinity differences between the two boxes were density compensated in the early period. The potential density of the deep mixed layers and deep isolated mixed layers was about 27.70 - 27.71 kg m^{-3} in the two boxes. In the north box, the density of those mixed layers increased to 27.72-27-73 kg m^{-3} at the end of the convective period and during the restratification phase. The few profiles available in the south box suggested that the potential density was between 27.1 and 27.2 kg m^{-3}. More profiles would be necessary in the south box to confirm the difference between the two boxes, which could be taken as further indirect evidence that the LSW found in the Irminger Sea was not entirely advected from the Labrador Sea, as suggested by Yashayaev et al. (2007) for instance.
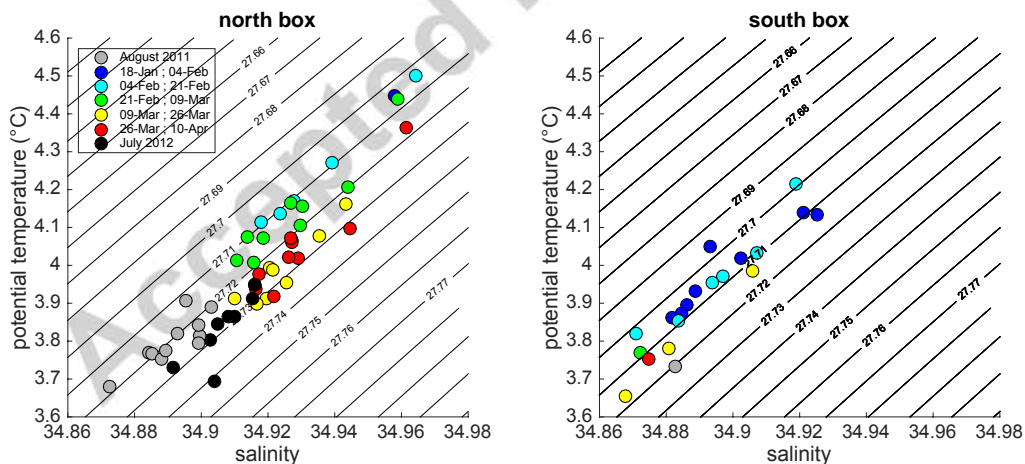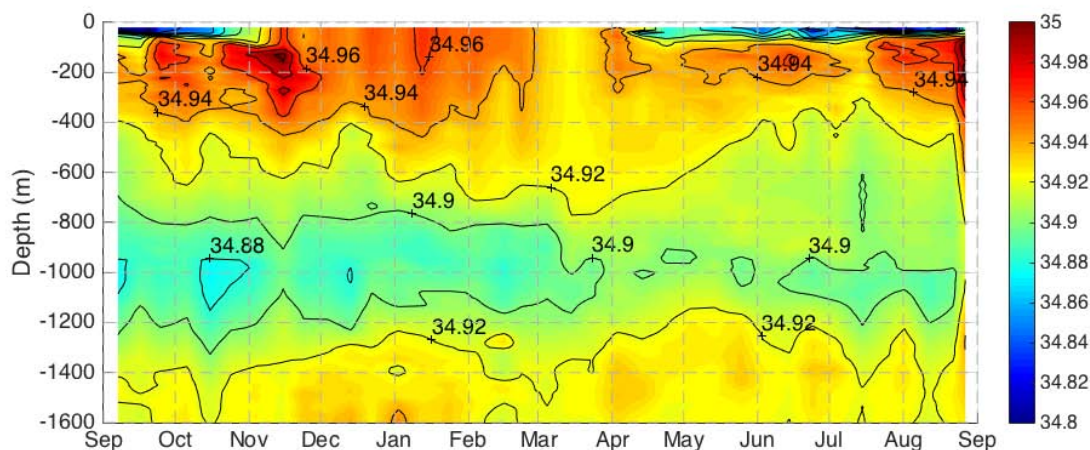
Figure 9: (Upper panels) θ/S properties in the north (left panel) and south (right panel) boxes of the deep mixed layer and the deep isolated mixed layers for 18 January - 4 February (cyan dots), 4 February- 21 February (blue dots), 21 February- 9 March (green dots), 9 March-25 March (yellow dots) and 25 March-10 April 2012 (red dots). Gray and black dots represent properties of the LSW found in the two boxes and averaged over 700-1000 m depth. The properties were estimated at the end of August 2011 from Argo profiles (gray dots) and in June-July 2012 from the hydrographic data collected along the Ovide line (Mercier et al., 2014). (Lower panel) Salinity time series in the north box based on all the Argo profiles available in the box and averaged over 15 day periods.

The salinity time series in the north box, based on Argo salinity profiles, clearly shows the presence of a salinity minimum centered near 1000 m depth and associated with the LSW core. The homogeneous salinity profiles down to nearly 1000 m mark the deep convection event that occurred in early March. Interestingly, the salinity of the LSW between 800 and 1000 m increased during this event and remained high until mid-June. This confirms that the deep convection observed during winter 2011-2012 in the Irminger Sea reached the LSW and partially modified its properties through the vertical redistribution of the salty waters found in the first hundred meters of the water column from September to February (Figure 9). The salinity of the LSW layer decreased after mid-June, which suggests the arrival of LSW from the Labrador Sea. Despite this partial renewal, the LSW found in the north box remained saltier and denser in summer 2012 than in summer 2011 (Figure 9).

The temporal evolution of the oxygen profiles from float 5902298 testifies to the local and rapid ventilation of the mixed layer by the deep convection (Figure 6d). Profiles collected between 30 January and 20 March showed oxygen saturation of about 94-96 % in the mixed layer. Such values are typical of deep overturning events (Reid, 1982) because the water is cooled and convected away from the sea surface at a much faster rate than oxygen can equilibrate between the surface waters and the atmosphere (Clarke and Coote, 1988). The oxygen saturation of the water masses lying below this upper layer was 85-90 %, indicating that the corresponding water masses were formed during preceding winters. From 30 January to 10 March, the depth of the 94-96% saturation layer increased from about 300 m to 1000 m. In addition, oxygen saturation for profiles collected from 19 February to 20 March was very homogeneous from the surface to 800 or 1000 m, demonstrating the on-going convective activity. After mid-March, the absence of convective activity was characterized by oxygen profiles that were less homogeneous vertically because of lateral intrusion or mixing with adjacent water masses (Körtzinger et al., 2003) and because near-surface restratification resulted in surface water saturation or even supersaturation due to biological activity (Figure 6d). No more profiles were available from float 5902298 after 9 April 2012.

3.2. Heat budget

To go further in the description of the deep convection that occurred during the winter of 2011-2012 in the Irminger Sea, a mixed layer heat budget was calculated along the trajectories of the 4 floats described previously, following de Boisséson et al. (2010). The heat budget was expressed as follows:

$$h\, \partial_t <T> = \frac{Fnet}{\rho_0 C_p} - U_E \partial_x T - V_E \partial_y T - [<T> - T(-h)] w_{ekman} \qquad (1)$$

22

where ρ_0 is the surface-referenced density, Cp is the heat capacity of the sea water, h is the

MLD, T is the potential temperature, <T> is the potential temperature averaged over h, Fnet is

the net air-sea heat flux, (U_E, V_E) are the eastward and northward components of the Ekman

horizontal transport and w_{ekman} is the vertical Ekman velocity. Equation 1 expresses the

balance between the heat content variation (HCV, lhs), the net air-sea fluxes (first term on

rhs), and the heat flux induced by the horizontal and vertical Ekman advection acting on

horizontal and vertical temperature gradients (last two terms on rhs). These terms are referred

to as the horizontal and vertical Ekman heat fluxes below. To derive this equation from the

one originally proposed by Caniaux and Planton (1998), a few assumptions were made and

are detailed by de Boisséson et al. (2010). We considered that the contributions to the mixed

layer temperature changes by the Ekman and the geostrophic flows were distinct and assumed

that the same mixed layer water mass was sampled in two consecutive profiles, which is

strictly true only in the absence of vertical shear in the horizontal velocity field. Hence, we

did not expect the Argo float, which drifted 1000 m over about 9 days and at the sea surface

over a few hours, to follow the mixed layer water mass perfectly. There was thus a

geostrophic advection contribution that could not be directly estimated along the trajectory of

the Argo float. To minimize the contribution of this unaccounted-for term, we followed the

procedure implemented by de Boisséson et al. (2010), who discarded consecutive Argo

profiles that clearly did not sample the same mixed layer water mass, for instance when float

4901163 showed an abrupt decrease in the MLD in February 2012 (Figure 7b). It was also

assumed that the Ekman layer was contained in the mixed layer, and SST data were thus used

to estimate the horizontal temperature gradients needed for the computation of the horizontal

Ekman heat flux. The vertical Ekman heat flux was expected to potentially play a role during

the preconditioning period but not during the convective period, as the thickness of the

Ekman layer did not exceed about 150 m (Wijffels et al., 1994). Finally, as in de Boisséson et

al. (2010), horizontal diffusion and vertical diffusion across the base of the mixed layer were neglected, as was advection of heat by horizontal velocity deviations from the mean.

The mixed layer heat budget was then estimated along the trajectories of the 4 floats from September 2011 to April or July 2012 depending on data availability. For each float, the 4 terms of the budget were calculated along the float trajectory between each profile and the one obtained 10 days later. For each pair of profiles, HCV was computed by considering a layer having a depth chosen as the deepest MLD of the two profiles (de Boisséson et al., 2010). The net air-sea heat fluxes and the SSTs were obtained directly from ERA-Interim while the Ekman horizontal transports and the vertical Ekman advection were derived from ERA-Interim wind fields (see Section 2.3). The net air-sea heat fluxes from NCEP and ARPEGE were also used to check the robustness of our results. Each term on the rhs of equation was interpolated on a daily basis at float profile positions determined assuming a rectilinear drift of the float at the parking pressure (de Boisséson et al., 2010).

As observed for the mixed layer deepening, the variations of heat content and the evolution of net air-sea fluxes were synchronous along each float trajectory (not shown). The heat budget terms of the 4 floats could thus be averaged because they were considered to be representative of this non-localized deep convection occurring at least at a regional scale (Figure 10). This averaging procedure smoothed the individual curves and provided more robust estimates of the different terms of the mixed layer heat budget. The three datasets gave similar results. At low frequency, the heat budget was nearly balanced by the HCV and net air-sea heat flux terms. From September to Mid-March, air-sea heat loss induced a cooling of the mixed layer. After mid-March, the net-air sea heat fluxes became positive, leading to a warming of the mixed layer. The amplitudes of those two main terms varied between 200 and -400 W m^{-2} (and even more with the NCEP heat fluxes). The horizontal and vertical Ekman heat fluxes varied between $\pm$ 10 W m^{-2} and between about $\pm$ 31 W m^{-2}, respectively. During the whole

24

period, they were one order of magnitude weaker than the net air-sea heat fluxes. Using heat fluxes estimated from ERA-Interim fields, the mean difference between HCV and the other three terms of the budget (Eq. 1) was 4.2 ± 19.4 W m^{-2}. The mean difference was larger when NCEP (17.4 ± 24.2 W m^{-2}) and ARPEGE (21.1 ± 19.8 W m^{-2}) were considered. The budget was closed within error bars with ERA-Interim and NCEP, which validates the assumptions made to derive Equation (1). This also suggests that the bias in the air-sea heat fluxes in the region is less than about 25 W m^{-2} and highlights the overall good quality of the heat fluxes in the subpolar gyre as also shown by de Boisséson et al. (2010) in the Iceland Basin. The amplitude of the standard errors reflects discrepancies observed on a monthly time scale between the net air-sea heat fluxes and the mixed layer heat content variations. Note, however, the agreement between the HCV and the net air-sea heat flux terms during the convective period in early March. During this period, heat loss was much larger in NCEP than in ERA-Interim or ARPEGE (Figure 5, Figure 10). The comparison with HCV suggests that the NCEP heat loss was overestimated.
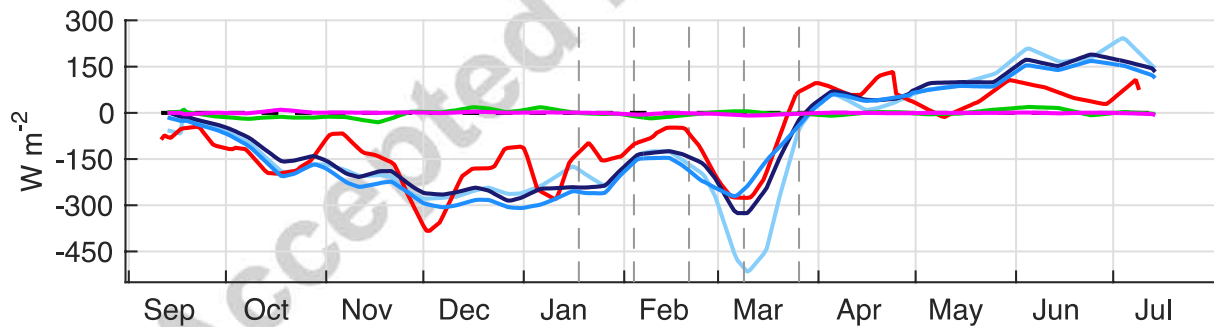

Figure 10: Mixed layer heat budget along the trajectories of floats 4901163, 4901165, 4901166 and 5902298, averaged for the 4 floats. (Red curves) Heat content variation (HCV). (Dark blue, cyan and blue curves) Net air-sea heat fluxes from ERA-Interim, NCEP and ARPEGE, respectively. (Green and magenta curves) Horizontal and vertical Ekman heat fluxes, respectively. A negative value corresponds to a heat loss by the mixed layer. The dashed vertical lines delimit periods identified in Figure 8, 18 January – 3 February, 4 February – 20 February, 21 February – 8 March and 9 March – 25 March.

At the end of the convective period (25 March 2012), the cumulated mixed layer heat content change since September 2011 was -25.9 x 10^8 J while the cumulated net air-sea heat fluxes reached -30.8 x 10^8 J, i.e. a difference between the two main terms of the heat budget of 4.9 x 10^8 J. About 17 % of this difference was explained by the Ekman terms, for which the cumulated values reached 0.7 x 10^8 J and -0.1 x 10^8 J for the horizontal and vertical heat transport divergence, respectively. The residual difference came from the neglected terms, from the assumptions made or errors in the atmospheric forcing, or from a combination of all of these.

To conclude, the mixed layer heat budget averaged along the trajectories of the 4 floats was closed within the error bars. this shows that the net air-sea heat fluxes were the main drivers of the mixed layer heat content variations along the float trajectories (Figure 10). Horizontal and vertical Ekman heat fluxes were of secondary importance in the budget.

3.3. Heat fluxes and role of the Greenland Tip Jets

We then investigated the mechanisms that led to the heat loss observed during winter 2011-2012. Given the agreement between the three air-sea flux datasets for the heat budget calculation (Section 3.2) and strong heat loss events (Figure 5), we consider only the ERA-Interim dataset in the following. Våge et al. (2008) showed the importance of strong intermittent wind events, such as the Greenland Tip Jets, for the development of a winter deep mixed layer in the Irminger Sea. Using ERA-interim wind and the Greenland Tip Jet detection criterion defined in Section 2.4, we estimated that 16 Greenland Tip Jet events occurred in the TJ box between 1 November 2011 and 30 April 2012 (Figure 11), the period considered by Våge et al. (2009b). Among those events, 3 lasted more than 24 hours and 2 of them considerably longer. Våge et al. (2009b) estimated that the mean duration of a Greenland Tip Jet in the period 1957-2002 was less than 24 hours and that there were, on

average, 13 ± 5 Greenland Tip Jets between November and April, the maximum being 20-25

Tip Jets. Considering those values, the winter of 2011-2012 was intense but not exceptional in

terms of number of Greenland Tip Jet events. However, the two events that occurred between

31 December and 2 January and between 5 and 9 March were of exceptional duration, lasting
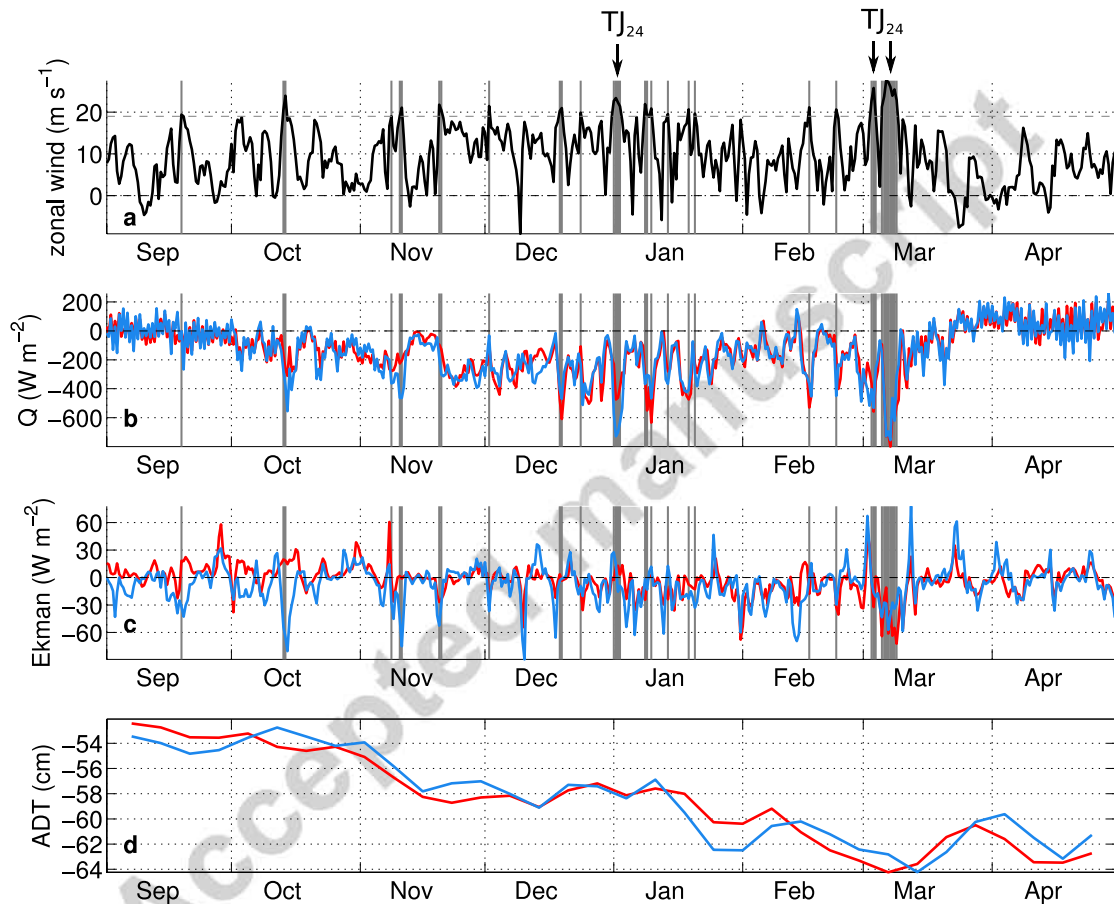
about 48 and 84 hours, respectively.

Figure 11: Time-series from 1 September 2011 to 30 April 2012 of (a) the maximum value of the zonal wind speed in the TJ box, (b) the net air-sea heat fluxes averaged over the north (red) and south (blue) boxes, (c) the horizontal and vertical Ekman heat fluxes averaged over the north (red) and south (blue) boxes (d) ADT averaged over the north (red) and south (blue) boxes (see Figure 1). The vertical bands correspond to zonal wind speed exceeding 19 m s^{-1}. TJ$_{24}$ identifies Greenland Tip Jet events longer than 24h.

The sequence of those events are compared to the net air-sea heat fluxes, the horizontal

Ekman heat fluxes and the ADT, averaged over the north and south boxes in Figure 11. The

vertical Ekman heat fluxes are neglected here as they are not expected to play a role during

winter, when the mixed layer is deeper than the Ekman layer. Because of the general storminess in the area, a net air-sea heat loss is observed in the two boxes from early October to the end of March. Most of the large heat loss events, identified by values typically greater than 400 W m^{-2} in the heat loss time series, are associated with a Greenland Tip Jet. In the north box, for instance, this is the case for 10 of the 11 large heat loss events. This confirms the dominant role of the Greenland Tip Jets to explain those large heat loss events. Most of the Greenland Tip Jets occurred in late December-early January and some of them were associated with a mean heat loss greater than 400 W m^{-2} (Figure 11b). Locally, the heat loss was even greater than 800 W m^{-2} in some cases (not shown). No Greenland Tip Jet was observed between mid-January and mid-February. Four Greenland Tip Jets were observed between mid-February and Mid-March. The last two Greenland Tip Jets were long and intense and were observed on 2-3 March and 5-9 March. The last Greenland Tip Jet was associated with a mean heat loss greater than 600 W m^{-2} (Figure 11b) in the two boxes and with locally extremely large heat loss of about 1000 W m^{-2} (not shown). For each Greenland Tip Jet, large heat losses are observed similarly in the two boxes (Figure 11b) with, however, some differences in the heat loss amplitude except for the last Greenland Tip Jet, for which the agreement between the two boxes was striking. The cumulated heat loss at the end of the convective period (25 March 2012) was very similar in the two boxes. It reached 29.4 x 10^8 J and 30.5 x 10^8 J in the north and south boxes, respectively.

When the horizontal Ekman heat fluxes were considered, the difference between the two boxes was larger than for the net air-sea heat fluxes (Figure 11c)), suggesting that the horizontal Ekman heat fluxes were associated with a smaller spatial scale than that of the net air-sea heat fluxes. The values of this term never exceeded ± 90 W m^{-2}. The term was negative in the two boxes during the last two Greenland Tip Jet events of early March, reaching about -70 W m^{-2} in both. During that period of time, the wind stress pattern led to an

Ekman-induced heat loss that reinforced (by about 10%) the heat loss induced by the net air-sea heat fluxes. The cumulated heat loss between 1 September and 25 March was one order of magnitude less than the heat loss amplitude induced by the net air-sea fluxes and reached 0.5 x 10^8 J and 1.4 x 10^8 J in the north and south boxes, respectively. These results complement previous findings from Pickart et al. (2003a) regarding the Ekman contribution to deep convection. Those authors showed that, in an idealized model of the deep convection in the Irminger Sea, the Ekman pumping preconditioned the water column as it decreased the thickness of the warm surface layer in the region where the buoyancy loss was maximum, reducing the heat to be removed during winter. They also showed that, with no wind stress in their idealized model, the final volume of ventilated water in their model was reduced by about 35%.

The winter heat loss gradually deepened the mixed layers from November to Mid-March. The apparition of the first deep mixed layer in early January followed the long Greenland Tip Jet event observed between 31 December 2011 and 2 January 2012 that was associated with intense heat loss. The absence of Greenland Tip Jet events between mid-January and mid-February coincided with reduced heat loss (Figure 11) and with a slowdown in the mixed layer deepening (Figure 8b). Finally, the two consecutive long and intense Greenland Tip Jets of early March coincided with the final deepening phase down to 1000 m. The large heat loss leading to this last deep convection event was due not only to the net air-sea heat fluxes but also to the horizontal Ekman heat fluxes, both being forced by the early March Greenland Tip Jets.

The mixed layer deepening induced by the winter heat loss from November to Mid-March was accompanied by a decrease in the ADT of about 10 cm in the three boxes between November and Mid-March (Figure 11d). The ADT reached a minimum at the end of the convective period.

To conclude, the role of the Greenland Tip Jet events was dominant in the mixed layer deepening in the Irminger Basin during winter 2011-2012. Although this winter was an average one in terms of number of Greenland Tip Jets, the two late events, exceptional in terms of duration and heat loss, played a crucial role in triggering the final mixed layer deepening phase, leading to the observed 1000 m deep mixed layers.

3.4. Interannual context

The interannual (1992-2013) context of the deep convection observed during winter 2011-2012 is now investigated on the basis of several indicators that we associate with the development of deep convection in the Irminger Sea. We first considered the number of Greenland Tip Jets per winter (Figure 4) together with the number of late (March) Greenland Tip Jets. The latter number was estimated from the monthly occurrence of high wind speed events in the TJ box calculated as the number of 12h wind fields for which the maximum wind speed in the TJ box exceeded 19 m s^{-1} (Figure 13).We also considered the ADT, the cumulated net air-sea heat fluxes and the cumulated horizontal Ekman heat fluxes. To be consistent with the Greenland Tip Jet estimates, the values were spatially averaged over the TJ box. We also considered the NAO index. It was in a highly positive state at the beginning of the nineties, shifted to a negative value in the winter 1995/1996 and has oscillated between positive and negative values since then (Figure 12d). After the 1995/1996 shift, the Irminger Sea became more stratified, as revealed by the ADT increase (Figure 12c), and the intensity and structure of the horizontal circulation in the Irminger Sea were modified (Häkkinen and Rhines, 2004; Våge et al., 2011).

In order to take the heat losses occurring from the beginning of autumn into account, a year was considered to run from 1 September to the following 31 August . For a given year, the heat fluxes were thus cumulated from 1 September to 31 August, after the mean annual cycle

had been removed from the time series calculated over 1992-2012 (Figure 12b,c). On average over 1992-2012, the net air-sea heat fluxes and the horizontal Ekman heat fluxes removed heat from the TJ box. The 1992-2012 mean cumulated air-sea heat flux peaked at about -24 x 10^8 J in March and then increased to -10 x 10^8 J in August. The 1992-2012 mean cumulated horizontal Ekman heat flux reached -0.5 x 10^8 J in March and increased to a value close to 0 in August. Interestingly, despite differences in the amplitude of the absolute values of those two terms, their anomalies were of the same order of magnitude: the Ekman contribution anomalies were about ± 2.3 x 10^8 J and the air-sea heat flux anomalies were about ± 8.8 x 10^8 J (Figure 12).

As for the heat fluxes, the mean annual cycle calculated over 1992-2012 was removed from the ADT time series (Figure 12c). We considered ADT as a proxy for the stratification of the water column. Low ADT anomaly in early September could be a sign of good preconditioning of the water column, which would be favorable to deep convection the following winter. Low ADT anomaly in March could be a sign of deep convection occurrence, although care must be taken in the interpretation of this signal (Gelderloos et al., 2013).

The values of these indicators for the winter of 2011-2012 were compared to those obtained for the winters of 1996-1997, 2007-2008 and 2008-2009, during which deep convection was directly observed or suggested by spring profiles (Bacon et al., 2003; Våge et al., 2008, de Jong et al., 2012). The comparison revealed that the winter of 2011-2012 was not exceptional compared to the other documented deep convective winters:

1. In all cases, the cumulated net air-sea heat flux anomalies were negative and thus favorable to deep convection. The air-sea heat loss of winter 2011-2012 was similar to that observed in the winter of 1996-1997. It lay between the largest air-sea heat loss observed in 2007-2008 and the more moderate heat loss observed in 2008-2009 (de Jong et al., 2012).

31

2. The cumulated horizontal Ekman heat flux anomalies were similar for winters 2007-2008, 2008-2009 and 2011-2012. They were negative, revealing that the heat loss in the TJ box due to the Ekman term was enhanced during those winters, which was also favorable to deep convection. During those winters, the contribution of the Ekman-induced heat loss anomaly to the total winter heat loss anomaly varied between 7 and 47%. Note that, in winter 1996-1997, the Ekman term contribution was close to the mean annual conditions (the anomaly was positive during winter and close to 0 in March).

3. Compared to the values observed after the 1995/1996 NAO shift, the ADT anomaly was rather low during the 4 winters in question. It was mostly positive during the winters of 2007-2008 and 2011-2012, while it was mostly negative during the winters of 1996-1997 and 2008-2009. The negative ADT anomaly values observed in 2008-2009 are consistent with de Jong et al.'s (2012) results that showed the crucial role of preconditioning in the development of deep convection that winter.

4. The winter of 2011-2012 was similar to that of 2007-2008 in terms of number of Greenland Tip Jets (17 and 16, respectively) (Figure 4) but it was similar to the winter of 1996-1997 in terms of late occurrence of high wind speed events (more than 10 occurrences in March) (Figure 13). Compared to those values, fewer Greenland Tip Jets were observed in winters 1996-1997 and 2008-2009 (12 and 11, respectively) and fewer high wind speed occurrences (only 5) were observed in March 2008 and 2009.

5. Finally, the NAO index was greater than one in each of those winters, except in 2008-2009 when the NAO was close to zero.

This comparison confirms that the development of deep convection in the Irminger Sea depends on various factors, such as strong heat loss, enhanced Ekman-induced heat loss, preconditioning, positive NAO index, and large number of Greenland Tip Jets, especially in

late winter. It also reveals the potential of those indicators to characterize deep convective winters, but none of them are either sufficient or necessary to detect deep convection occurrence in the Irminger Sea. For instance, the Ekman term was not favorable to deep convection in 1996-1997; the moderate air-sea heat loss was not favorable to deep convection in 2008-2009 (de Jong et al., 2012); the preconditioning as measured by the ADT was not crucial for the occurrence of deep convection in 2007-2008 (Våge et al. 2009a, de Jong et al. 2012) or in 2011-2012.

Further investigations are thus required to refine the use of those indicators, which are not completely independent. For example, more Greenland Tip Jets are generally observed during positive NAO years (Pickart et al., 2003a). However, we can speculate that deep convection occurred when the six indicators were favorable to it. This was the case for the winter of 1992-1993 (Figure 12,13). Similarly, we can speculate that deep convection did not occur when none of the indicators were favorable. This was the case for the winter of 2009-2010, for which de Jong et al. (2012) showed that no deep convection occurred.
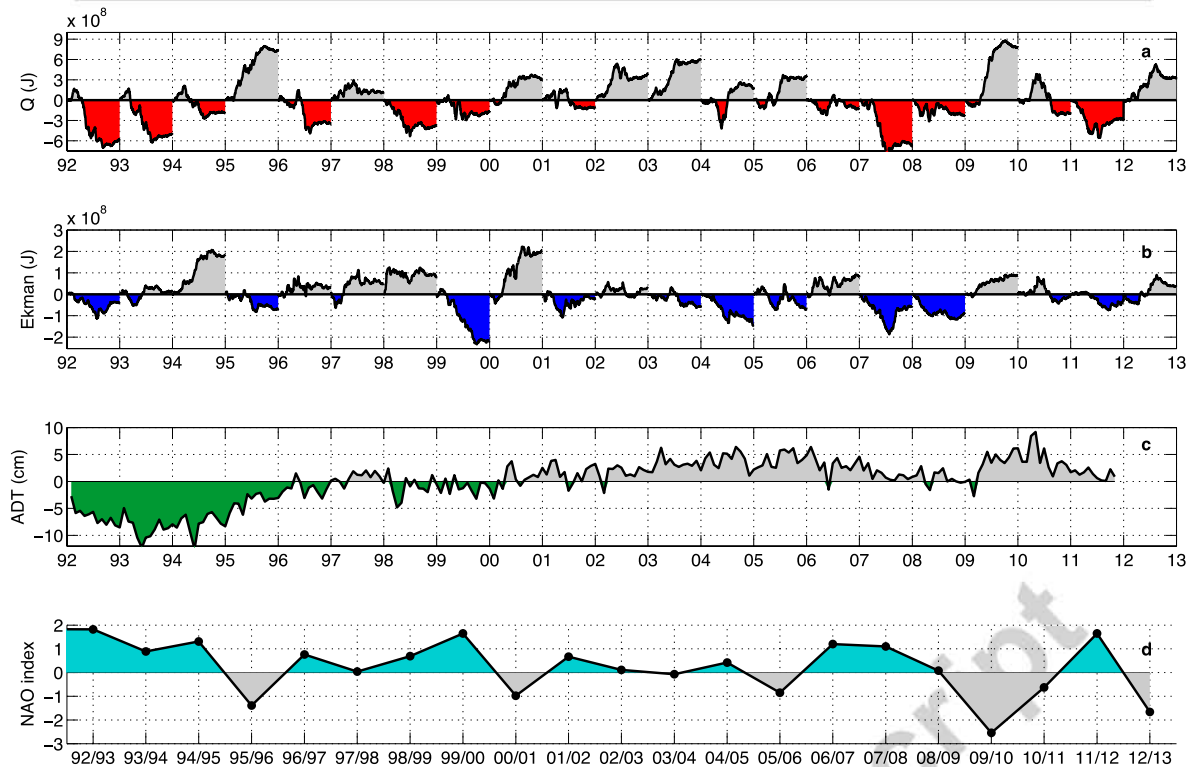
Figure 12: (a, b, c) Time series over 1992-2013 of anomalies with respect to a mean annual cycle estimated over the same period of (a) net air-sea heat fluxes cumulated from 1 September to 31 August of the following year, (b) horizontal Ekman heat fluxes cumulated from 1 September to 31 August of the following year and (c) ADT (cm). Fields are averaged in the TJ box. (d) Time series of the Hurrell PC-based North Atlantic Oscillation wintertime (DJFM) index from 1992 to 2013.
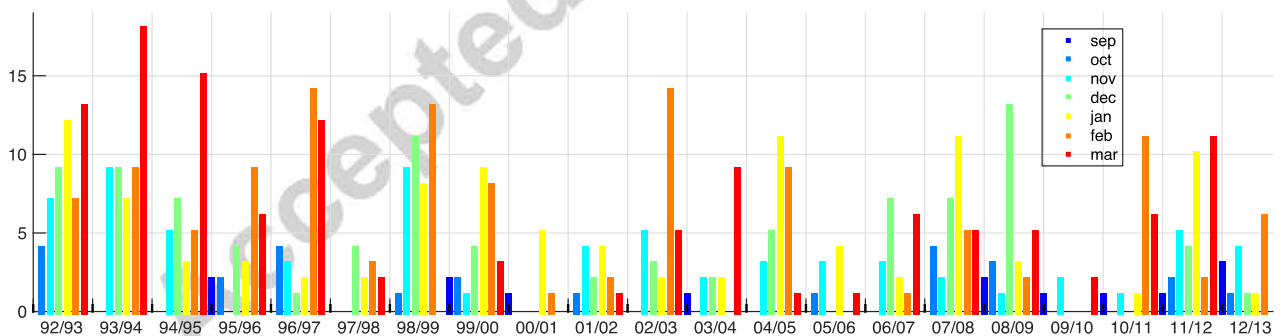

Figure 13: Monthly occurrence, from September to March for the years 1992-2013, of high wind speed events in the TJ box calculated as the number of 12h wind fields for which the maximum zonal wind speed in the TJ box exceeds 19 m s^{-1} in ERA-Interim. Note that consecutive maximum zonal wind fields are counted separately here while they are considered as part of the same Greenland Tip Jet event in Figure 11.

To conclude, deep convection in the Irminger Sea is not a rare isolated event: over the last

two decades, deep convection has occurred in at least 4 winters. Positive NAO index, strong

34

heat loss due to net air-sea heat fluxes, enhanced Ekman-induced heat loss, preconditioning of the water column, and late Greenland Tip Jet events are conditions favorable to deep convection in the Irminger Sea. However, none of them is either sufficient or necessary. When those indicators are considered, the 2011-2012 event was not exceptional compared to the other documented deep convective events. Its particularity, besides the exceptional spatial sampling, lay in the long and intense Greenland Tip Jets that occurred in March and that pushed the mixed layer deepening down to 1000m. The other well document events were associated with other particularities: a southward shift in the storm tracks and an extended ice cover in the Labrador Sea in 2007-2008 (Våge et al., 2008) or good preconditioning in 2008-2009 including a large number of Greenland Tip Jets in November 2008 (de Jong et al., 2012).

4. Conclusions

Analysis of Argo data for the winter of 2011-2012 revealed the presence of an exceptionally large number of profiles (41) over the Irminger Basin with MLDs exceeding 700 m, which was deep enough to reach the pool of intermediate Labrador Sea Water located in the Irminger Sea. Among them, 4 profiles exhibited an MLD of 1000 m, which was the maximum value observed for that winter. A large number of spring profiles (17) also presented an isolated mixed layer deeper than 700 m, which reached 1000 m for 5 of them. The depth reached by the deep convection is similar to that observed since 1997 in a few localized profiles (Bacon et al., 2003; Våge et al., 2009a; de Jong et al., 2012). The deep profiles were mainly observed in the eastern part of the Irminger Gyre characterized by the -55 cm ADT contour.

Thanks to the Argo array, which provided profiles for the whole Irminger Sea during the winter of 2011-2012, the different phases of the mixed layer deepening leading to deep convection down to 1000 m, were observed, with their spatial extent, for the first time in the

Irminger Sea. This was possible because the sampling in the Irminger Sea in winter 2011-2012 was 3 to 4 times that performed in preceding winters. For instance, the number of profiles available between January and April in a box where the Greenland Tip Jets were the most intense (the Tip Jet box, Figure 1) was 36 in 2012, while it was 9 on average over 2002-2010.

The deepening phase occurred in various steps. Two intense convective periods occurring in late January south of Cape Farewell and in late February-early March east of Greenland were separated by a period (early February) characterized by less intense convective activity. A final deepening period was observed in mid-March, during which the deepest mixed layers were observed (1000 m). This long deepening period was followed by a rapid restratification phase. The deepening of the mixed layer occurred in large regional areas. It is not impossible that the mixed layer deepening occurred simultaneously over a single large area extending from the south of Cape Farewell to the center part of the Irminger Gyre, as suggested by the few profiles exhibiting deep mixed layers east of Greenland in January and south of Cape Farewell in late February-mid March. This reveals that, although the sampling of the Irminger Sea by Argo floats during winter 2011-2012 was exceptional, even denser and more uniform sampling would be needed for a full description of the spatial pattern of deep convection in this Sea. This pleads in favor of better Argo sampling in both time and space in the Irminger Sea and, more generally, in the subpolar gyre of the North-Atlantic to cope with its high interannual and spatial variability. This could be achieved through the use of a moored frame that could release floats at a predetermined date or when triggered by an event such as a temperature, salinity or oxygen anomaly.

The θ/S properties of the deep mixed layers and the deep isolated mixed layers were warmer and saltier in the northern part of the convective area (east of Greenland) than in the southern part (south of Cape Farewell). Temperature and salinity differences between the two areas are

density compensated during the deepening phase and the potential density of the mixed layers evolved from about 27.70 - 27.71 kg m^{-3} in early January to about 27.71-27-73 kg m^{-3} at the end of the convective period. The temporal evolution of the oxygen profiles from float 5902298 testifies to the local, rapid ventilation of the mixed layer by the deep overturning events. In early March, very homogeneous oxygen saturation of 94-96% was observed from the surface to 800 or 1000 m, demonstrating the on-going convective activity.

A mixed layer heat budget along the trajectories of the 4 floats that sampled the deepest mixed layers showed that heat loss at the air-sea interface was mainly responsible for the heat content variations in the mixed layer. Greenland Tip Jet events enhanced the winter heat loss and two long (more than 24 hours), intense late events close together in time pushed the mixed layer deepening down to 1000 m. They occurred at a period of the year generally characterized by the beginning of restratification.

As revealed by this and earlier studies, the indicators pertinent for assessing whether conditions are favorable for the development of deep convection in the Irminger Sea are: the net air-sea fluxes, the number of Greenland Tip Jets, especially in late winter, the stratification of the water column represented by the Absolute Dynamic Topography, the NAO index and the horizontal Ekman heat fluxes. During a deep convective event, the contribution of the Ekman-induced heat loss anomaly can be as large as 47 % of the total winter heat loss anomaly. When these indicators were considered, the 2011-2012 event was not significantly different compared to the other documented deep convective events. None of the indicators is either sufficient or necessary for detecting the occurrence of deep convection in the Irminger Sea. It is also impossible to know in advance the volume of dense water masses formed by convection as it depends on the uncertainties associated with synoptic scale atmospheric conditions, particularly at the pivotal time at the end of the long period of winter preconditioning.

It is now clear that deep convection in the Irminger Sea is not a rare isolated event as deep convection has occurred in 4 winters over the last two decades. It is thus time to move forward and to investigate the contribution of the Irminger Sea to the volume of dense water masses formed in the North-Atlantic Ocean, to the MOC, and more generally, to the ventilation of the intermediate layers. The questions to be addressed include the impact of the variability of deep convection occurrence in the Irminger Sea on the MOC variability or on the oceanic oxygen uptake (Maze et al., 2012), which is a useful quantity to improve our comprehension of the global carbon cycle (Bopp et al., 2002).

part of the Global Ocean Observing System. We thank A. Bentamy (LOS/IFREMER) for

providing ASCAT data. The NAO data were downloaded from the UCAR Climate Data

Guide website (Schneider et al., 2013): https://climatedataguide.ucar.edu/climate-data/hurrell-

north-atlantic-oscillation-nao-index-pc-based.

5. References

Bacon, S., Gould, W. J., and Jia, Y., 2003. Open-ocean convection in the Irminger Sea. Geophys. Res. Lett., 30(5), 1246. doi:10.1029/2002GL016271.

Bentamy, A., Croize-Fillon, D., Perigaud, C., 2008. Characterization of ASCAT measurements based on buoy and QuikSCAT wind vector observations. Ocean Sci., 4(4), 265–274. doi:10.5194/os-4-265-2008.

Bentamy, A., Grodsky, S. A., Carton, J. A., Croizé-Fillon, D., Chapron, B., 2012. Matching ASCAT and quikSCAT winds. J. Geophys. Res., 117, C02011. doi:10.1029/2011JC007479.

Bopp, L., Quéré, C. L., Heimann, M., Manning, A. C., and Monfray, P.: Climate-induced oceanic oxygen fluxes: Implications for the contemporary carbon budget, Global Biogeochem. Cy., 16, 1022–1045, doi:10.1029/2001GB001445, 2002.

Caniaux, G., Planton, S., 1998. A three-dimensional ocean mesoscale simulation using data from the SEMAPHORE experiment : Mixed layer heat budget. J. Geophys. Res., 103, C11, 25081–25099. doi:10.1029/98JC00452.

Centurioni, L. R., Gould, W. J., 2004. Winter conditions in the Irminger Sea observed with profiling floats. J. Mar. Res. 62, 313–336. doi:10.1357/0022240041446209.

Clarke, R. A., Gascard, J.-C., 1983. The Formation of Labrador Sea Water. Part I: Large-Scale Processes, J. Phys. Oceanogr., 13, 1764–1778. doi:10.1175/1520-0485(1983)013<1764:TFOLSW>2.0.CO;2.

Clarke, R. A. and A. R. Coote., 1988. The Formation of Labrador Sea Water. Part III: The Evolution of Oxygen and Nutrient Concentration, J. Phys. Oceanogr., 18, 469-480.

de Boisséson, E., Thierry, V., Caniaux, G., 2010. Mixed layer heat budget in the Iceland Basin from Argo. J. Geophys. Res., 115, C10055. doi:10.1029/2010JC006283.

de Boyer Montégut, C., Madec, G., Fischer, A. S., Lazar, A., Iudicone, D., 2004. Mixed layer depth over the global ocean : An examination of profile data and a profile-based climatology. J. Geophys. Res., 109, C12003. doi:10.1029/2004JC002378.

Dee, D. P., Uppala, S. M., Simmons, A. J., Berrisford, P., Poli, P., Kobayashi, S., Andrae, U., Balmaseda, M. A., Balsamo, G., Bauer, P., Bechtold, P., Beljaars, A. C. M., van de Berg, L., Bidlot, J., Bormann, N., Delsol, C., Dragani, R., Fuentes, M., Geer, A. J., Haimberger, L., Healy, S. B., Hersbach, H., Holm, E. V., Isaksen, L., Kallberg, P., Kohler, M., M. Matricardi, A. P. M., Monge-Sanz, B. M., Morcrette, J. J., Park, B. K., Peubey, C., de

Rosnay, P., Tavolato, C., Thépaut, J.-N., Vitart, F., 2011. The ERA-Interim reanalysis: configuration and performance of data assimilation system. Q. J. R. Meteorol. Soc., 137, 553-597. doi:10.1002/qj.828

de Jong, M. F., van Aken, H. M., Vage, K., Pickart, R. S., 2012. Convective mixing in the central Irminger Sea: 2002-2010. Deep-Sea Res. I, 63, 36–51. doi :10.1016/j.dsr.2012.01.00.

Déqué, M., Dreveton, C., Braun, A., Cariolle, D., 1994. The Arpege/Ifs Atmosphere Model: a Contribution to the French Community Climate Modeling. Clim. Dyn., 10, 249–266. doi:10.1007/BF00208992.

Dickson R., Lazier, J., Meincke, J., Rhines, P., Swift, J., 1996. Long-term coordinated changes in the convective activity of the North-Atlantic. Prog. Oceanogr., 38, 241-295.

Doyle, J. D., Shapiro, M. A., 1999. Flow response to large-scale topography: the Greenland tip jet. Tellus A, 51, 728–748. doi: 10.1034/j.1600-0870.1996.00014.x.

Gaillard F., Autret, E., Thierry, V., Galuap, P., Coatanoan, C., Loubrieu, T., 2009. Quality Control of Large Argo Datasets. J. Atmos. Ocean. Technol., 26, 337-351. doi: 10.1175/2008JTECHO552.1

Gelderloos, R., C. A. Katsman, and K. Våge, 2013. Detecting Labrador Sea Water formation from space, J. Geophys. Res. Oceans, *118*, 2074–2086, doi:10.1002/jgrc.20176.

Harden, B. E., I. A. Renfrew, G. N. Petersen, 2011. A Climatology of Wintertime Barrier Winds off Southeast Greenland. J. Climate, 24, 4701-4717. doi:10.1175/2011JCLI4113.1.

Häkkinen, S., and P. B. Rhines, 2004, Decline of Subpolar North Atlantic Circulation during the 1990s, Science, 304, 555– 559.

Hurrell, J. W., 1995. Decadal Trends in the North Atlantic Oscillation: Regional Temperature and Precipitation. Science, 269, 676–679, doi:10.1126/science.269.5224.676.

Kanamitsu, M., Ebisuzaki, W., Woollen, J., Yang, S. –K., Hnilo, J. J. , Fiorino, M., Potter, G. L., 2002. NCEP–DOE AMIP-II Reanalysis (R-2). Bull. Amer. Meteor. Soc., 83, 1631–1643. doi:10.1175/BAMS-83-11-1631.

Körtzinger, A. , Schimanski, J., Send, U., Wallace, D., 2004. The Ocean Takes a Deep Breath, Science, 306, 1337. doi:10.1126/science.1102557.

Lazier, J. R. N., 1980. Oceanographic conditions at Ocean Weather Ship Bravo, 1964-1974. Atmosphere-Ocean, 18:3, 227-238. doi:10.1080/07055900.1980.9649089.

Lazier, J., Pickart, R., Rhines, P., 2001. Deep convection. In: Siedler, G., Church, J., Gould, J., Ocean Circulation and Climate: Observing and Modelling the Global Ocean. International Geophysics Series, San Diego, vol. 77, pp. 387-400. doi:10.1016/S0074-6142(01)80130-3.

Lherminier P., Mercier H., Gourcuff C., Alvarez M., Bacon S., Kermabon C., 2007. Transports across the 2002 Greenland-Portugal Ovide section and comparison with 1997. J. Geophys. Res.-Oceans, 112, C07003. doi: 10.1029/2006JC003716.

Luo D., Yao, Y., Feldstein, S. B., 2014. Regime Transition of the North Atlantic Oscillation and the Extreme Cold Event over Europe in January–February 2012. Mon. Wea. Rev., 142,

4735-4757. doi: 10.1175/MWR-D-13-00234.1.

Marshall, J., Schott, F., 1999. Open-ocean convection: observations, theory, and models. Rev. Geophys., 37, 1–64. doi: 10.1029/98RG02739.

Maze G., H. Mercier, V. Thierry, L. Memery, P. Morin, and F. F. Perez, 2012. Mass, nutrient and oxygen budgets for the northeastern Atlantic Ocean. Biogeosciences, 9, 4099–4113, doi:10.5194/bg-9-4099-2012

Mercier, H., P. Lherminer, A. Sarafanov, F. Gaillard, N. Daniault, D. Desbruyères, A. Falina, B. Ferron, T. Huck, V. Thierry, 2015. Variability of the meridional overturning circulation at the Greenland–Portugal OVIDE section from 1993 to 2010. Prog. Oceanogr. (2013), http://dx.doi.org/10.1016/j.pocean.2013.11.001

Moore, G. W. K., 2003. Gale force winds over the Irminger Sea to the east of Cape Farewell, Greenland. Geophys. Res. Lett., 30, 1894. doi:10.1029/2003GL018012.

Moore, G. W. K., Renfrew, I. A., 2005. Tip Jets and Barrier Winds : a QuikSCAT Climatology of High Wind Speed Events around Greenland. J. Climate, 18, 3713-3727. doi:10.1175/JCLI3455.1.

Moore, G. W. K., 2012. A new look at Greenland flow distortion and its impact on barrier flow, tip jets and coastal oceanography. Geophys. Res. Lett., 39, L22806. doi:10.1029/2012GL054017.

Moore, G. W. K., 2014. Mesoscale Structure of Cape Farewell Tip Jets. J. Climate, 27, 8956-8965.

Nansen, F. 1912. Das Bodenwasser und die Abkuhlung des Meeres. Int. Rev. Gesamten Hydorbiologie und Hydrographie Band V 1, 1–42.

Owens, W.B., Wong, A. P. S., 2009. An improved calibration method for the drift of the conductivity sensor on autonomous CTD profiling floats by Ɵ-S climatology. Deep-Sea Res. I, 56, 450–457. doi:10.1016/j.dsr.2008.09.008.

Pickart, R. S., Torres D. J., Clarke R. A., 2002. Hydrography of the Labrador Sea during Active Convection. . Phys. Oceanogr., 32, 428-457.

Pickart, R. S., Spall, M. A., Ribergaard, M. H., Moore, G. W. K., Milliff, R. F., 2003a. Deep Convection in the Irminger sea forced by the Greenland tip jet. Nature, 424, 152–156. doi:10.1038/nature01729.

Pickart, R.S., Straneo, F., Moore, G.W.K., 2003b. Is Labrador Sea Water formed in the Irminger Basin? Deep Sea Res. I, 50, 23–52. doi:10.1016/S0967- 0637(02)00134-6.

Pickart, R. S., D. J. Torres, and P. S. Fratantoni, 2005. The East Greenland Spill Jet. J. Phys. Oceanogr., 35, 1037–1053.

Reid, J. L., 1982. On the use of dissolved oxygen concentration as an indicator of winter convection, Naval Res. Rev., 34, 28– 39.

Renfrew, I. A., Moore, G. W. K., Holt, T. R., Chang, S. W., Guest, P., 1999. Mesoscale Forecasting during a Field Program: Meteorological Support of the Labrador Sea Deep Convection Experiment. Bull. Amer. Meteor. Soc., 80, 605-620. doi:10.1175/1520-

0477(1999)080<0605:MFDAFP>2.0.CO;2.

Renfrew, I. A., Petersen, G. N., Sproson, D. A. J., Moore, G. W. K., Adiwidjaja, H., Zhang, S., North, R., 2009. A comparison of aircraft-based surface-layer observations over Denmark Strait and the Irminger Sea with meteorological analyses and QuikSCAT winds. Q. J. R. Meteorol. Soc., 135, 2046-2066. doi: 10.1002/qj.444.

Rogers, J. C., 1990. Patterns of Low-Frequency Monthly Sea Level Pressure Variability (1899–1986) and Associated Wave Cyclone Frequencies. J. Climate, 3, 1364–1379. doi:10.1175/1520-0442(1990)003<1364:POLFMS>2.0.CO;2.

Schneider, D. P., Deser, C., Fasullo, J., Trenberth, K. E., 2013. Climate Data Guide Spurs Discovery and Understanding. Eos Trans. AGU, 94(13), 121. doi: 10.1002/2013EO130001.

Sproson, D. A. J., Renfrew, I. A., Heywood, K. J., 2008. Atmospheric conditions associated with oceanic convection in the south-east Labrador Sea. Geophys. Res. Lett., 35, L06601. doi:10.1029/2007GL032971.

Sverdrup, H.U., Johnson, M.W., Fleming, R.H., 1942. The Oceans: Their Physics, Chemistry, and General Biology, Prentice-Hall, Inc., Englewood Cliffs, NJ. USA.

Sy, A., Rhein, M., Lazier, J. R., Koltermann, K. P., Meincke, J., Putzka, A., Bersch, M., 1997. Surprisingly rapid spreading of newly formed intermediate waters across the North Atlantic Ocean. Nature, 386, 675-679. doi:10.1038/386675a0.

Takeshita, Y., Martz, T. R., Johnson, K. S., Plant, J. N., Gilbert, D., Riser, S. C., Neill, C. Tilbrook, B., 2013. A climatology-based quality control procedure for profiling float oxygen data. J. Geophys. Res. Oceans, 118, 5640–5650. doi:10.1002/jgrc.20399.

Thomson, R. E., Fine, I. V., 2003. Estimating Mixed Layer Depth from Oceanic Profile Data. J. Atmos. Oceanic Technol., 20, 319-329. doi:10.1175/1520-0426(2003)020<0319:EMLDFO>2.0.CO;2.

Uppala, S. M., Kållberg, P. W., Simmons, A. J., Andrae, U., Bechtold, V. D. C., Fiorino, M., Gibson, J. K., Haseler, J., Hernandez, A., Kelly, G. A., Li, X., Onogi, K., Saarinen, S., Sokka, N., Allan, R. P., Andersson, E., Arpe, K., Balmaseda, M. A., Beljaars, A. C. M., Berg, L. V. D., Bidlot, J., Bormann, N., Caires, S., Chevallier, F., Dethof, A., Dragosavac, M., Fisher, M., Fuentes, M., Hagemann, S., Hólm, E., Hoskins, B. J., Isaksen, L., Janssen, P. A. E. M., Jenne, R., Mcnally, A. P., Mahfouf, J.-F., Morcrette, J.-J., Rayner, N. A., Saunders, R. W., Simon, P., Sterl, A., Trenberth, K. E., Untch, A., Vasiljevic, D., Viterbo, P., Woollen, J., 2005. The ERA-40 re-analysis. Q.J.R. Meteorol. Soc., 131: 2961–3012. doi: 10.1256/qj.04.176.

Våge, K., Pickart, R. S., Moore, G. W. K., Ribergaard, M. H., 2008. Winter Mixed Layer Development in the Central Irminger Sea : The Effect of Strong, Intermittent Wind Events. J. Phys. Oceanogr., 38, 541-565. doi:10.1175/2007JPO3678.1.

Våge, K., Pickart, R. S., Thierry, V., Reverdin, G., Lee, C. M., Petrie, B., Agnew, T. A., Wong, A., Ribergaard, M. H., 2009a Surprising return of deep convection to the subpolar North Atlantic Ocean in winter 2007-2008. Nat. Geosci., 2, 67–72. doi:10.1038/ngeo382.

Våge, K., Spengler, T., Davies, H. C., Pickart, R. S., 2009b. Multi-event analysis of the westerly Greenland tip jet based upon 45 winters in ERA-40. Q.J.R Meteorol. Soc., 135, 1999–2011. doi: 10.1002/qj.488.

Våge, K., Pickart, R. S., Sarafanov, A., Knutsen, O., Mercier, H., Lherminier, P., van Aken, H. M., Meincke, J., Quadfasel, D., Bacon, S., 2011. The Irminger Gyre : Circulation, convection, and interannual variability. Deep Sea Res. I, 58(5), 590-614. doi:10.1016/j.dsr.2011.03.001.

Visbeck, M., Chassignet, E. P., Curry, R. G., Delworth, T. L., Dickson, R. R., Krahmann, G., 2003. The ocean's response to North Atlantic Oscillation variability. In: Hurrel, J. W., Kushnir, Y., Ottersen, G., Visbeck, M., The North Atlantic Oscillation: Climatic Significance and Environmental Impact. American Geophysical Union, Washington, D. C., vol. 134, pp. 113– 146. doi :10.1029/134GM06.

Wijffels, S., Firing, E., Bryden, H., 1994. Direct Observations of the Ekman Balance at 10°N in the Pacific. *J. Phys. Oceanogr.*, 24, 1666–1679. doi:10.1175/1520-0485(1994)024<1666:DOOTEB>2.0.CO;2.

Wong A., Keeley, R., Carval, T. and the Argo Data Management Team, 2014. Argo Quality Control Manual. doi:10.13155/33951.

Wu, C. F. J., Hamada, M., 2000. Experiments: planning, analysis, and parameter design optimization. Wiley ed., ISBN: 978-0-471-69946-0, 760 p.

Yashayaev, I., Bersch, M., van Aken, H. M., 2007. Spreading of the Labrador Sea Water to the Irminger and Iceland basins. Geophys. Res. Lett., 34, L10602. doi:10.1029/2006GL028999.

Highlights

- Exceptional Argo sampling in the Irminger Sea during winter 2011-2012

- 41 profiles with MLD greater than 700 m; MLD of 1000 m for 4 of them

- First description of the spatial extent of deep convection in the Irminger Sea

- Heat loss at the air-sea interface main contributor to mixed layer deepening

- Air-sea heat loss enhanced by Greenland Tip Jets and Ekman contribution